

RESEARCH

Open Access



Systematic in vitro analysis of therapy resistance in glioblastoma cell lines by integration of clonogenic survival data with multi-level molecular data

Leon Emanuel Schnöller¹, Daniel Piehlmaier², Peter Weber^{2,3}, Nikko Brix¹, Daniel Felix Fleischmann^{1,4,5}, Alexander Edward Nieto¹, Martin Selmsberger², Theresa Heider², Julia Hess^{2,3}, Maximilian Niyazi^{1,4,6}, Claus Belka^{1,3,4,6}, Kirsten Lauber^{1,3,4}, Kristian Unger^{2,3*†} and Michael Orth^{1*†}

Abstract

Despite intensive basic scientific, translational, and clinical efforts in the last decades, glioblastoma remains a devastating disease with a highly dismal prognosis. Apart from the implementation of temozolomide into the clinical routine, novel treatment approaches have largely failed, emphasizing the need for systematic examination of glioblastoma therapy resistance in order to identify major drivers and thus, potential vulnerabilities for therapeutic intervention. Recently, we provided proof-of-concept for the systematic identification of combined modality radiochemotherapy treatment vulnerabilities via integration of clonogenic survival data upon radio(chemo)therapy with low-density transcriptomic profiling data in a panel of established human glioblastoma cell lines. Here, we expand this approach to multiple molecular levels, including genomic copy number, spectral karyotyping, DNA methylation, and transcriptome data. Correlation of transcriptome data with inherent therapy resistance on the single gene level yielded several candidates that were so far underappreciated in this context and for which clinically approved drugs are readily available, such as the androgen receptor (AR). Gene set enrichment analyses confirmed these results, and identified additional gene sets, including reactive oxygen species detoxification, mammalian target of rapamycin complex 1 (MTORC1) signaling, and ferroptosis/autophagy-related regulatory circuits to be associated with inherent therapy resistance in glioblastoma cells. To identify pharmacologically accessible genes within those gene sets, leading edge analyses were performed yielding candidates with functions in thioredoxin/peroxiredoxin metabolism, glutathione synthesis, chaperoning of proteins, prolyl hydroxylation, proteasome function, and DNA synthesis/repair. Our study thus confirms previously nominated targets for mechanism-based multi-modal glioblastoma therapy, provides proof-of-concept for this workflow of multi-level data integration, and identifies novel candidates for which pharmacological inhibitors are readily available and whose targeting in combination with radio(chemo)therapy deserves further examination. In addition, our study also reveals that the presented workflow requires mRNA expression data, rather

[†]Kristian Unger and Michael Orth have equally contributing senior authors

*Correspondence:

Kristian Unger
unger@helmholtz-muenchen.de

Michael Orth
michael.orth@med.uni-muenchen.de

Full list of author information is available at the end of the article



© The Author(s) 2023. **Open Access** This article is licensed under a Creative Commons Attribution 4.0 International License, which permits use, sharing, adaptation, distribution and reproduction in any medium or format, as long as you give appropriate credit to the original author(s) and the source, provide a link to the Creative Commons licence, and indicate if changes were made. The images or other third party material in this article are included in the article's Creative Commons licence, unless indicated otherwise in a credit line to the material. If material is not included in the article's Creative Commons licence and your intended use is not permitted by statutory regulation or exceeds the permitted use, you will need to obtain permission directly from the copyright holder. To view a copy of this licence, visit <http://creativecommons.org/licenses/by/4.0/>. The Creative Commons Public Domain Dedication waiver (<http://creativecommons.org/publicdomain/zero/1.0/>) applies to the data made available in this article, unless otherwise stated in a credit line to the data.

than genomic copy number or DNA methylation data, since no stringent correlation between these data levels could be observed. Finally, the data sets generated in the present study, including functional and multi-level molecular data of commonly used glioblastoma cell lines, represent a valuable toolbox for other researchers in the field of glioblastoma therapy resistance.

Keywords Glioblastoma, Therapy resistance, Multi-level molecular data, Correlation analysis

Introduction

Glioblastoma, despite immense efforts in preclinical, translational, and clinical research during the last decades still remains a daunting disease with highly dismal prognosis [1]. Fractionated radio(chemo)therapy with 30 fractions of 2 Gy and concomitant administration of DNA-alkylating temozolomide (TMZ) in definitive or adjuvant settings, followed by TMZ-based maintenance therapy remains the standard of care [2, 3]. However, glioblastoma is well-known for its high degree of inherent therapy resistance, both to ionizing radiation (IR) and TMZ, resulting in frequent treatment failure and early recurrence [4]. Thus, a more detailed understanding of the biological and molecular mechanisms underlying glioblastoma therapy resistance is needed in order to open new perspectives for molecularly targeted therapy and to improve disease prognosis [5, 6].

Based on our recent proof-of-concept study [7], we here present a systematic approach which integrates inherent resistance data of commonly used human glioblastoma cell lines to IR and TMZ with multi-level molecular data of those cell lines obtained under treatment-naïve conditions, including spectral karyotyping (SKY FISH), array comparative genomic hybridization (aCGH), array-based DNA methylation, and transcriptomic (mRNA microarray) analyses. By integrating these data with scores of inherent therapy resistance as extracted by dimensionality reduction of clonogenic survival data ([7, 8], Additional file 1: Table S1), and subsequent gene set enrichment analysis (GSEA) [9], we could identify several candidate networks and signaling circuits which are associated with inherent treatment resistance of glioblastoma cells and can be readily targeted by clinically approved or at least clinically trialed drugs. Among these were pathways involved in homeostasis of reactive oxygen species (ROS), mammalian target of rapamycin complex 1 (mTORC1) signaling, and androgen receptor (AR) signaling [10, 11]. Taken together, we present a novel integrative approach for the systematic identification of therapeutic vulnerabilities (not only) in glioblastoma as well as potential candidates whose targeting in conjunction with radiotherapy and/or TMZ may help to break glioblastoma therapy resistance.

Methods

Cell culture

The human glioblastoma cell lines A172, LN18, LN229, T98G, U87 [12], U138, and U251 were purchased from the American Type Culture Collection (ATCC, Manassas, VA, USA), or from Cell Lines Service GmbH (CLS, Eppelheim, Germany), and confirmed for identity by short tandem repeat (STR) typing according to the standards of the ATCC and the American National Standards Institute (ANSI, New York, NY, USA) of 2011 (ANSI/ATCC ASN-0002–2011) [13]. All cell lines were cultured in Dulbecco's Modified Eagle Medium (D-MEM) supplemented with 10% (v/v) heat-inactivated fetal calf serum (FCS), 100 U/ml penicillin, and 0.1 mg/mL streptomycin (all from Thermo Scientific, Schwerte, Germany) at 37 °C and 7.5% CO₂. Cells were kept at low passage numbers (≤ 10 passages), and were regularly tested by MycoAlert assay (Lonza, Basel, Switzerland) to be free of mycoplasma contamination.

Determination of therapy resistance scores

Resistance to therapy was determined by clonogenic survival assays as described [7]. In brief, cells were seeded into 6-well plates and incubated for 4 h in order to adhere. Cells were irradiated at the indicated doses in single-shot or in intervals of 24 h (fractionated mode), and colony formation was allowed for up to 12 d. In case of TMZ treatment, cells were incubated with TMZ at the indicated doses for 24 h, medium was changed, and colony formation was performed in TMZ-free medium. For the combination treatment, cells were exposed to 5 μ M TMZ for 24 h, irradiated at the indicated doses, and incubated in TMZ-free medium for colony formation. Colonies were fixed with 80% ethanol, stained with 0.8% methylene blue (both from Merck Millipore, Darmstadt, Germany), and counted with a Stemi 305 stereomicroscope (Carl Zeiss, Oberkochen, Germany) as described [7, 14]. Percentages of colony forming cells were calculated and normalized to the respective plating efficiencies at approximately matched colony numbers. Resistance scores were extracted by principal component analysis (PCA) as scores of the first principal component (PC1) [8].

Spectral karyotyping (SKY FISH)

For spectral karyotyping (SKY FISH) analyses, cells at 80% confluency were accumulated in M-phase by treatment with 0.1 µg/ml colcemid (Roche Diagnostics, Basel, Switzerland) for 3 h. Cells were then harvested with TrypLE Express (Thermo Scientific), and incubated in 4.0% (w/v) potassium chloride for 45 min at 37 °C. Cells were fixed with fixative (methanol and glacial acetic acid at 3:1 ratio, both from Merck Millipore) for 45 min at 4 °C, washed, and resuspended in fixative. Cell suspensions were dripped onto microscope slides, and hybridization was performed using the denatured SKY-probe mixture kit SkyPAINT DNA (Applied Spectral Imaging, Carlsbad, CA, USA) as previously described [15]. For staining, slides were incubated with anti-digoxigenin (Roche), avidin-Cy5, and avidin-Cy5.5 antibodies (Biomol, Hamburg, Germany), and counterstained with 0.1% (w/v) 4',6-diamidino-2-phenylindole (DAPI, Sigma-Aldrich, Taufkirchen, Germany). Slides were supplemented with Vectashield mounting solution (Vector Laboratories, Burlingame, CA, USA), and spectral imaging was performed with a Zeiss AxioPlan 2 fluorescence microscope (Carl Zeiss, Oberkochen, Germany) equipped with a SpectraCube device and SkyView software (both from Applied Spectral Imaging). Description of karyotypes was performed according to the international system of human cytogenetic nomenclature (ISCN, edition 2013) [16].

Global gene expression microarrays

To analyze global mRNA expression levels in glioblastoma cells, gene expression microarray analysis was performed. In brief, total RNA was extracted from cells using the Qiagen Allprep DNA/RNA mini kit (Qiagen). RNA concentration was determined with a Nanodrop ND-1000 spectrophotometer (Thermo Scientific), and RNA quality was assessed by a total RNA 6000 nano chip assay performed on an Agilent 2100 Bioanalyzer (Agilent Technologies, Santa Clara, CA, USA). To obtain global mRNA expression data, 50 ng of total RNA was subjected to Agilent SurePrint G3 human 8 × 60 k V2 microarray analysis (AMADID 039,494, Agilent Technologies). RNA from untransformed human astrocytes (Provitro AG, Berlin, Germany) served as reference. Results were collected using the Agilent feature extraction software (version 10.7, Agilent Technologies), and exported as text files. Assessment of data quality, filtering, and data processing were performed with the Bioconductor R packages Limma and Agi4 × 44PreProcess as previously described [17], and data analysis was performed with R. The obtained data are available at Gene

Expression Omnibus (GEO, super set accession number: GSE119637) and under the link <https://www.ncbi.nlm.nih.gov/geo/query/acc.cgi?acc=GSE119637> using the token 'sfqnocumrvofrmv'.

Array comparative genomic hybridization (aCGH)

To identify genomic copy number alterations (CNAs) in glioblastoma cells, array comparative genomic hybridization (aCGH) analyses were performed as previously described [18]. In brief, DNA was extracted from cells by Qiagen Allprep DNA/RNA mini kit (Qiagen), concentration and quality of DNA were assessed with a Nanodrop ND-1000 spectrophotometer (Thermo Scientific), and 120 ng DNA was fluorescently labelled using the CYTAG SuperCGH labelling kit (Enzo Life Sciences, New York, NY, USA). After removing free nucleotides using Microcon YM-30 columns (Merck Millipore), labelled DNA was subjected to oligonucleotide-based high-resolution SurePrint G3 Human 60 k CGH microarray analysis (AMADID 021,924, Agilent Technologies). Microarrays were scanned with a G2505C SureScan microarray scanning system (Agilent Technologies), raw data were extracted using the Agilent feature extraction software (version 10.7, Agilent Technologies), and CNA regions were identified using the Bioconductor R packages CGHcall and CGHregions [18, 19]. A compilation of all molecular data collected in this study is deposited as an Excel file in the Additional file 2.

Array-based DNA methylation analyses

Array-based DNA methylation analyses were performed as previously described [7]. In brief, DNA was extracted by Qiagen Allprep DNA/RNA mini kit (Qiagen), concentration and quality of DNA were assessed with a Nanodrop ND-1000 spectrophotometer (Thermo Scientific), and 500 ng DNA was subjected to hybridization on an Infinium EPIC methylation array (Illumina, San Diego, CA; USA). The arrays were scanned, idat files were imported in R using the minfi package [20], and processed in accordance to the Illumina BeadStudio data analysis workflow (Illumina). Beta values were used for downstream hierarchical clustering analysis along with the beta values retrieved for glioblastoma samples from TCGA database <https://www.cancer.gov/tcga> [21, 22].

Comparison of transcriptome and methylome profiles of glioblastoma cell lines with those from glioblastoma and lower-grade glioma (LGG) patient samples

Transcriptome profiles and methylome beta values from glioblastoma and LGG patient samples were retrieved from TCGA (https://tcga-data.nci.nih.gov/docs/publications/lgggbm_2015/) [21, 22]. Transcriptome profiles

of 560 glioblastoma and 463 LGG patients were corrected for putative batch effects and z-scaled per gene before combination with the transcriptomic data obtained from the cell lines in a common gene expression matrix. The top 20 differently expressed genes between glioblastoma and LGG samples were analyzed by hierarchical clustering (Fig. 1b, clustering method ward.D and euclidean distance measure), and principal component analysis (PCA).

For DNA methylation, the profiles of 410 glioblastoma and 516 LGG patients were included, and a merged beta value matrix including the methylation profiles of glioblastoma and LGG patients as well as those of the glioblastoma cell lines matching the CpG

island methylator phenotype (CIMP) signature by Ceccarelli et al. [21] was generated. The methylation profiles were subjected to hierarchical clustering analysis (Fig. 1c, clustering method ward.D and euclidean distance measure), and analyzed by PCA.

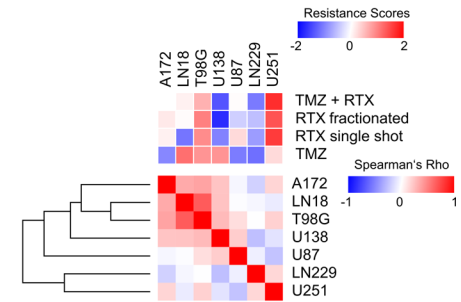
Molecular subtyping based on cytogenetic and transcriptomic data

Molecular subtyping was performed via different approaches. For calculation of molecular subtype scores (Additional file 1: Table S3), the data derived from cytogenetic characterization (SKY FISH) and aCGH analyses together with the expression data of relevant driver genes were utilized. All molecular subtype features of a cell line

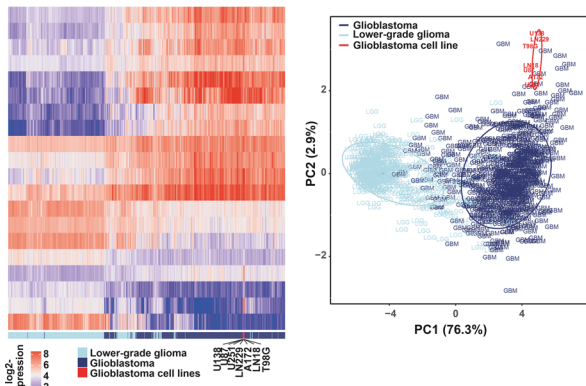
A

	A172	LN18	T98G	U138	U87	LN229	U251
RRID	CVCL_0131	CVCL_0392	CVCL_0556	CVCL_0020	CVCL_0022	CVCL_0393	CVCL_0021
Sex	male	male	male	male	male	female	male
Age	53 years	61 years	61 years	47 years	unspecified	60 years	75 years
Population	Caucasian	Caucasian	Caucasian	Caucasian	Caucasian	Caucasian	Caucasian
IDH1	wildtype	wildtype	wildtype	wildtype	wildtype	wildtype	wildtype
P53		mutant (C238S)	mutant (M237I)	mutant (R213Q)		mutant (P98L)	mutant (R273H)
MGMT promoter methylation	positive	negative	weak	negative	positive	positive	weak
MGMT mRNA expression	negative	positive	positive	positive	negative	negative	weak

D



B



C

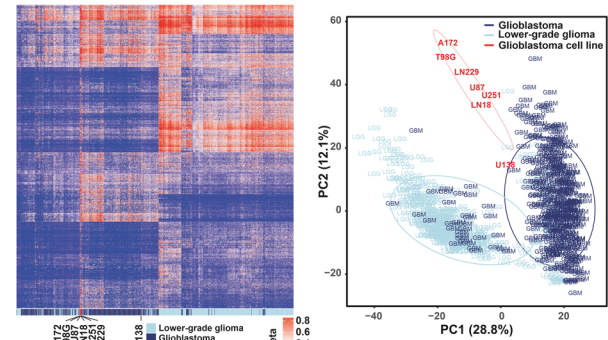


Fig. 1 Sample-to-sample correlation of mRNA expression of 100 most differently expressed genes in a human glioblastoma cell line panel does not match with inherent therapy resistance **a** Tabular presentation of characteristics of the human glioblastoma cell lines as obtained from the Cellosaurus database (<https://web.expasy.org/cellosaurus/>). **b** Unsupervised hierarchical clustering and principal component analysis (PCA) of mRNA expression levels of top 20 genes differently expressed between glioblastoma and low-grade glioma (LGG) patient samples (data from the TCGA database (https://tcga-data.nci.nih.gov/docs/publications/lgggbm_2015/), clustering method ward.D and euclidean distance measure) in 560 glioblastoma and 463 LGG patient samples, and in glioblastoma cell lines. **c** Unsupervised hierarchical clustering and PCA of G-CIMP signatures for hypermethylation phenotypes in 410 glioblastoma and 516 LGG patient samples (data from the TCGA database), and in glioblastoma cell lines. **d** Sample-to-sample correlation analysis of mRNA expression of 100 genes with highest intra-panel variation in expression in human glioblastoma cell lines. Expression values were determined by global gene expression microarray analysis. PCA-derived scores of inherent resistance (PC1s as described in [7, 8]) to single-shot radiotherapy (RTX), fractionated RTX, TMZ, and TMZ + single-shot RTX are depicted on top by unsupervised hierarchical clustering

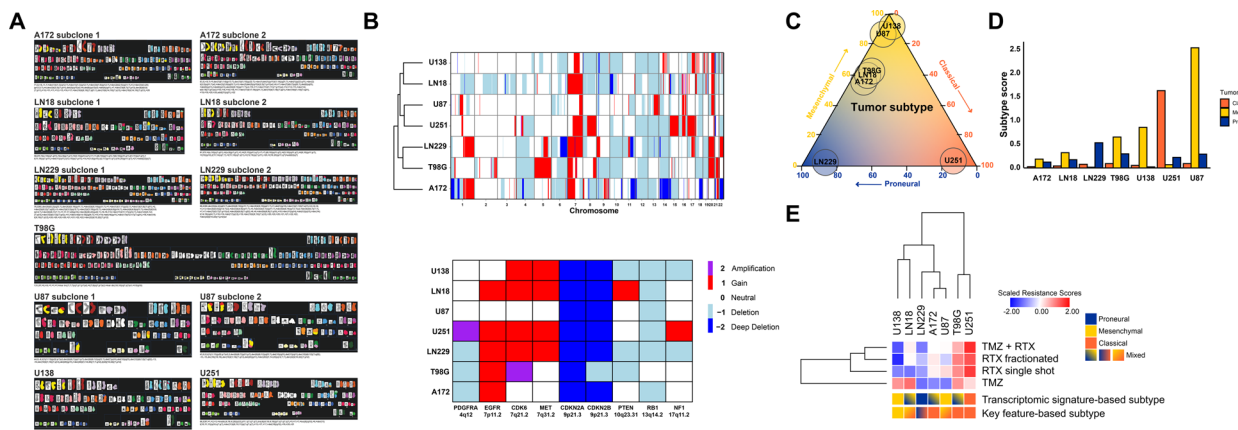


Fig. 2 Molecular subtyping of human glioblastoma cell lines. **a** Spectral karyotyping (SKY FISH) analyses of human glioblastoma cell lines. SKY FISH analyses were performed as previously described [15]. Karyotypes were described according to the international system of human cytogenetic nomenclature (ISCN, edition 2013) [16]. For cell lines A172, LN18, LN229, and U87, two distinct cytogenetic subclones are shown each. **b** Array comparative genomic hybridization (aCGH) analysis of glioblastoma cell lines. Hierarchical clustering of genomic copy number calls of chromosomes 1–22 in glioblastoma cell lines (top), and copy number status of gene loci with known association to glioblastoma subtypes (bottom). Copy number gains (up to 4 copies) are depicted by red bars, copy number amplifications (> 4 copies) by purple bars, and copy number losses by light blue (1 copy), and dark blue (complete loss), respectively. **c** Ternary plot of molecular subtyping of human glioblastoma cell lines on basis of mRNA expression of subtype-related signature genes (according to Wang et al. [23]), obtained by ssGSEA. The proneural subtype is depicted in blue, the classical subtype is depicted in orange, and the mesenchymal subtype is depicted in yellow. Values for subtypes were scaled to sum of 100% per cell line. **d** Bar plots of molecular subtype scores. **e** Graphical presentation of molecular subtypes of human glioblastoma cell lines as revealed by transcriptomic signature-based (top) and key feature-based subtyping (bottom), respectively. Scores of inherent therapy resistance are depicted by unsupervised hierarchical clustering

were summed up before being divided by the total number of features (Fig. 2c). Alternatively, molecular subtyping was performed by the single-sample gene set enrichment analysis (ssGSEA) algorithm provided as an R-package by Wang et al. [23], and using the reduced transcriptomic signatures from Verhaak et al. [24] (Fig. 2d). The negative log₁₀ values of the resulting p-values were used as molecular subtype scores, and according to the maximum value the molecular subtype was assigned.

Integration of therapy resistance with microarray expression data

Integration of therapy resistance data with microarray transcriptome data was performed via different alternative approaches. On single gene level, log₂ expression values obtained by microarray analyses were subjected to Pearson's correlation with resistance scores as extracted from clonogenic survival data via PCA (Additional file 1: Table S1 and [7, 8]). Similarly, but with focus on cancer-related genes, only members of the cancer gene consensus (CGC), a library of genes stored in the catalogue of somatic mutations in cancer (COSMIC) [25] were used for correlation analyses. Thirdly, integration on gene set level was performed by ranking genes in accordance to their respective correlation coefficients with therapy resistance scores followed by pre-ranked gene set enrichment analyses (GSEAs) [9]. Leading edge genes

were visualized by functional interaction networks in Cytoscape (Cytoscape Consortium, San Diego, CA, USA) [26]. Lastly, integration on gene set level was alternatively performed via an inverse workflow in which the complexity of microarray expression data was first reduced by gene set variation analysis (GSVA) [26] in single samples, followed by Pearson's correlation analyses with therapy resistance scores.

Results

Major differences in global mRNA expression patterns do not match with scores of inherent therapy resistance in a panel of human glioblastoma cell lines

The high degree of therapy resistance, the dismal prognosis, and the persisting lack of prognostic and/or predictive factors in glioblastoma demand for the identification of novel stratification markers for treatment responses on one hand, and potential vulnerabilities for combined modality strategies on the other [6, 27, 28]. Very recently, we published a proof-of-concept screen in which scores of inherent treatment resistance of glioblastoma cells, both to IR and TMZ (Additional file 1: Table S1), were correlated with basal mRNA expression levels of genes related to the DNA damage response (DDR)—a promising target to undermine therapy resistance in glioblastoma [7]. We were able to identify several DDR genes

whose mRNA expression levels showed significant positive correlation with inherent therapy resistance, and pharmacological interference with the function of some of the corresponding gene products using specific inhibitors indeed resulted in sensitization of resistant glioblastoma cells to IR or TMZ treatment, respectively [7].

In the present study, we expanded this workflow to the global transcriptomic level and performed gene expression and DNA methylation microarray analyses using the same cell line panel as before (Fig. 1a, [7]). We first employed the transcriptome/methylome profiles of the cell lines to analyze their relatedness to clinical tumor samples, either from glioblastoma or from lower-grade glioma (LGG) patients as available from TCGA (Fig. 1b, c). All glioblastoma cell lines clustered closer to the glioblastoma patient samples than to the LGG samples, both on the transcriptome (Fig. 1b) and the methylome level (Fig. 1c). However, the cell lines were located at the periphery of the glioblastoma sample cluster, indicating a traceable but limited relatedness which may derive from the absence of non-tumor cells in the cell lines, adaptation processes in cell culture, or other reasons, respectively. We next examined whether the most striking transcriptomic differences across the cell line panel can be linked to inherent therapy resistances of glioblastoma cells. However, sample-to-sample correlation analyses on basis of the 100 most differentially expressed genes resulted in clusters of cell lines without obvious associations to therapy resistance (Fig. 1d). As an example, LN18 and T98G cells, the two most closely related cell lines according to sample-to-sample correlation of their expression profiles revealed strong differences in their respective levels of treatment resistance (Fig. 1d, and [7]) which was most obvious for regimens encompassing IR. Vice versa, cell lines with similar levels of treatment resistance, for instance A172 and U87, showed very far relatedness in sample-to-sample correlation of their gene expression profiles (Fig. 1d). Thus, inherent therapy resistance of glioblastoma cells cannot be directly linked to major differences in global mRNA expression patterns, at least in the cell line panel we analyzed here. Obviously, more systematic approaches integrating large-scale molecular (OMICs) data with functional data are needed [4].

Multi-level cytogenetic and molecular characterization of human glioblastoma cell lines allows their classification into defined molecular subtypes

Several classification systems of glioblastoma on different molecular levels have been described [29]. Emerging consensus is the categorization according to genomic and transcriptomic features into three defined subtypes, termed the classical, the proneural, and the

mesenchymal subtype [23, 24]. Model systems of these subtypes have been reported to exhibit marked differences in the response to therapy in vitro and in vivo [30, 31], and the mesenchymal subtype was found to be the most refractory. Intriguingly, strong phenotypic plasticity between subtypes could be observed [30, 31], and the transition from the proneural to the mesenchymal subtype was described to be an important driver of therapeutic failure [30–32]. Clinically, the mesenchymal subtype exhibits the most dismal and the proneural subtype the most benign prognosis, suggested to be driven by subtype-specific signaling pathways including DNA damage repair, cell cycle control, mesenchymal cell movement, mitogen-activated protein kinase (MAPK)/extracellular signal-regulated kinase (ERK) signaling, PI3K/AKT signaling, JAK/STAT signaling, and WNT pathways [23, 29, 33].

We therefore aimed to classify the glioblastoma cell lines of our panel according to these described subtypes. Firstly, we performed spectral karyotyping (SKY FISH) analyses (Fig. 2a and Additional file 1: Table S2). The karyotypes ranged from a near-diploid chromosomal content in U87 cells up to a near-hexaploid one found in T98G (Fig. 2a and Additional file 1: Table S2). We also noticed that some of the cell lines (A172, LN18, LN229, T98G, and U87) displayed different cytogenetic subclones (Fig. 2a and Additional file 1: Table S2) which is indicative for enhanced chromosomal instability (CIN) in these cell lines [34]. Increased CIN, in turn, is known to affect all major aspects of cancer pathogenicity including tumor progression, metastasis formation, and therapy resistance [35–37], and this also holds true for glioblastoma [38, 39]. Mechanistically, elevated CIN leads to gene copy number alterations (CNAs), which in case of affecting oncogenic driver genes can give rise to the aforementioned subtypes [40, 41]. Distinct CNAs were shown to be associated with different molecular subtypes [24, 42, 43], and we therefore performed array comparative genomic hybridization (aCGH) analyses (Fig. 2b and Additional file 1: Table S3). CNAs with documented association to the classical subtype, including amplification of 7p11.2 (EGFR), and focal deletions of 9p21.3 (CDKN2A) [24], were detected in most of the cell lines (Fig. 2b and Additional file 1: Table S3), whereas CNAs with association to the mesenchymal (loss of 17p11.2, NF1) or the proneural subtype (amplification of 4q12, PDGFRA) were only rarely detected. According to our transcriptomic analyses, driver genes of the mesenchymal subtype, such as TRADD, RELB, TNFRSF1A, and CASP1 [24, 42], were widely expressed. On the contrary, expression of genes related to the proneural subtype including NKX2-2, OLIG2, SOX2, and ERBB3 [24, 44–46] was only detected in one cell line given by LN229

(Additional file 1: Table S3), and genes linked to the classical subtype such as NOTCH3, NES, and SMO [47] were expressed heterogeneously across our panel. In synopsis, subtyping on the basis of cytogenetic and transcriptomic key features classified cell lines A172, T98G, and U251 as classical, and U138 as mesenchymal, but failed to deliver clear-cut classifications for cell lines LN18, LN229, and U87 (Fig. 2e and Additional file 1: Table S3).

Subtyping on the basis of transcriptomic signature genes according to Wang et al. [23] revealed a more heterogeneous pattern of subtypes across our cell line panel (Fig. 2c-e). For A172, LN18, and T98G no clear-cut classifications could be obtained (denoted as "mixed"). These cell lines were located on the proneural-mesenchymal axis (Fig. 2c), presumably reflecting the aforementioned plasticity in proneural-mesenchymal transition. For LN229, U87, U138, and U251, on the contrary, clear-cut classifications could indeed be achieved, classifying LN229 as proneural, U251 as classical, and U87 and U138 as resembling the prognostically challenging mesenchymal subtype (Fig. 2c-e). Reasons for the slight prevalence of this subtype among the panel could be excessive clonal selection and adaptation during initial establishment, and long-term cultivation of these cell lines.

Integrating global gene expression data with clonogenic survival data as a strategy to identify new markers of glioblastoma therapy resistance

So far, our study has revealed that the annotation of defined molecular subtypes to established glioblastoma cell lines is challenging and yields different results depending on the molecular level and the key features employed. Furthermore, our data show that no direct association between the degree of therapy resistance and major transcriptomic differences or molecular subtypes can be drawn. Cell lines assigned to the highly treatment-refractory mesenchymal subtype (U138, U87) showed modest (U87) or even high (U138) sensitivity towards therapy, while the cell line U251 representing the classical subtype showed highest resistance (Fig. 2e). We therefore subjected the therapy resistance data and the transcriptomic profiling data of our glioblastoma cell line panel to correlation analyses with different workflows ([7], and Fig. 3). Firstly, utilizing whole transcriptome data, remaining on the single gene level, and setting a cutoff of $|R| \geq 0.9$ for the correlation of therapy resistance scores and log₂ microarray expression values disclosed a limited set of genes whose expression levels were associated with resistance against IR and/or TMZ treatment. Most strikingly, the highest positive correlation for TMZ treatment ($R > 0.99$) was seen for O⁶-methylguanine-DNA-methyltransferase (MGMT), not only confirming the literature [48, 49], but also

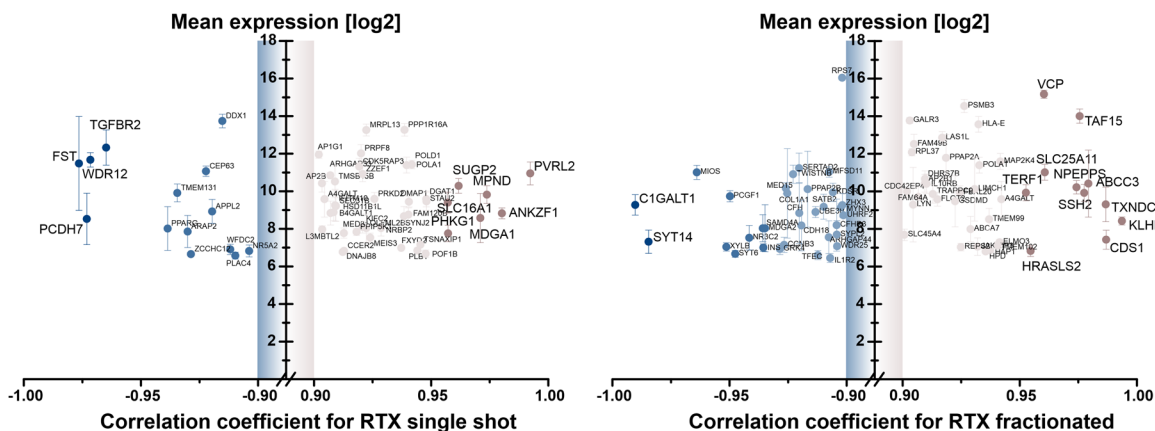
providing a very strong proof-of-concept for the feasibility of our methodological approach.

This strategy allowed us to identify 14 genes that exhibited significant positive correlation with inherent resistance to at least two of the four tested treatments ([7], and Fig. 3a, b), and 8 genes showing negative correlation (Fig. 3b and Additional file 1: Table S4). Three of the positively correlating genes were even linked to resistance towards three of the four treatments, including single-shot IR, fractionated IR, and single-shot IR plus TMZ (Fig. 3a, b). These genes encoded for alpha-1,4-galactosyltransferase (A4GALT), DNA polymerase alpha 1 (POLA1), a replication-associated DNA polymerase for which specific inhibitors are currently developed [50], and adaptor related protein complex 2 subunit beta 1 (AP2B1).

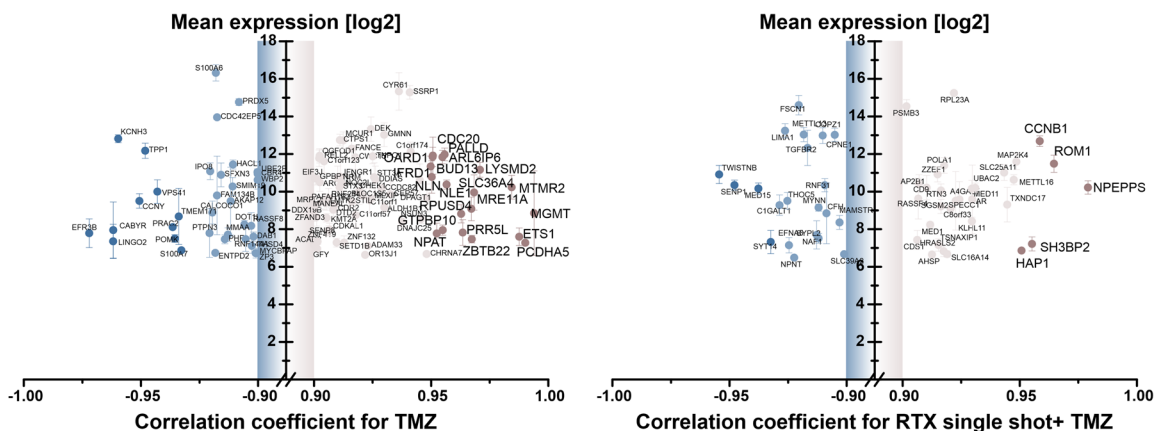
In order to focus on cancer-related genes, we next took advantage of the Cancer Gene Consensus (CGC) gene collection, which encompasses 1133 genes with documented functions in development and progression of cancer [25]. Using this compilation of reduced complexity compared to the whole transcriptome microarray and lowering the cut-off to $|R| \geq 0.7$ yielded a total of 27 cancer-related genes with positive, and 29 genes with negative correlation with resistance scores for at least two types of treatment (Fig. 4a, b). For more detailed analyses, we concentrated on genes, whose expression levels correlated with resistance against three types of treatment, resulting in 22 genes in total, 11 with positive correlation, and 11 with negative correlation (Fig. 4a, b). We then performed a search for drugs targeting the respective gene products with positive correlation with inherent therapy resistance (Fig. 4a and Additional file 1: Table S5). The most interesting target with the strongest expression dynamics across the cell line panel as identified by this approach was the androgen receptor (AR) which has recently been reported to play an important role in prognosis and therapy resistance of glioblastoma [51–57]. Since AR also has roles in other cancer entities, mostly in prostate and in breast cancer [58, 59], multiple inhibitors and antagonists of AR have been developed and trialed [60], yielding successful therapeutic targeting of the AR in these cancer entities [61, 62]. Another candidate for which targeted drugs with clinical approval in other cancer entities are readily available was the mitogen-activated protein kinase kinase 4 (MAP2K4) [63]. Interestingly, in case of glioblastoma a link between AR and MAPK signaling with regard to therapy resistance has recently been described [64]. Finally, our correlation analyses identified STAT5B as a druggable target [65, 66] whose expression was associated with therapy resistance, yet with rather low expression dynamics across the glioblastoma cell line panel.

A

Correlation with resistance to RTX single shot Correlation with resistance to RTX fractionated



Correlation with resistance to TMZ Correlation with resistance to RTX single shot+ TMZ



B

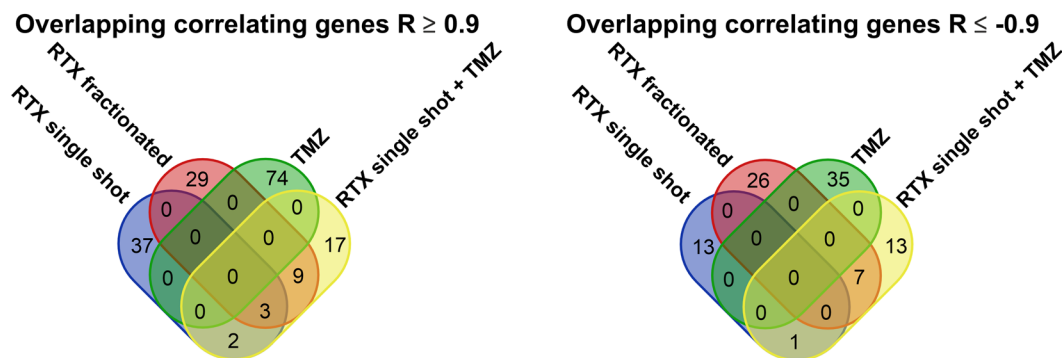


Fig. 3 Integration of global mRNA expression data with scores of inherent therapy resistance in human glioblastoma cell lines. **a** Graphical representation of genes whose log2 mRNA expression levels show strong positive or negative correlation ($|R| \geq 0.9$) with inherent resistance to single-shot RTX, fractionated RTX, TMZ, and single-shot RTX + TMZ in human glioblastoma cell lines. Only genes with an average log2 expression value of 6 or higher compared to astrocytes are shown. **b** Intersect analysis of genes whose log2 mRNA expression shows significant positive or negative correlation ($|R| \geq 0.9$) with inherent resistance to single-shot RTX (blue), fractionated RTX (red), TMZ (green), and single-shot RTX + TMZ (yellow)

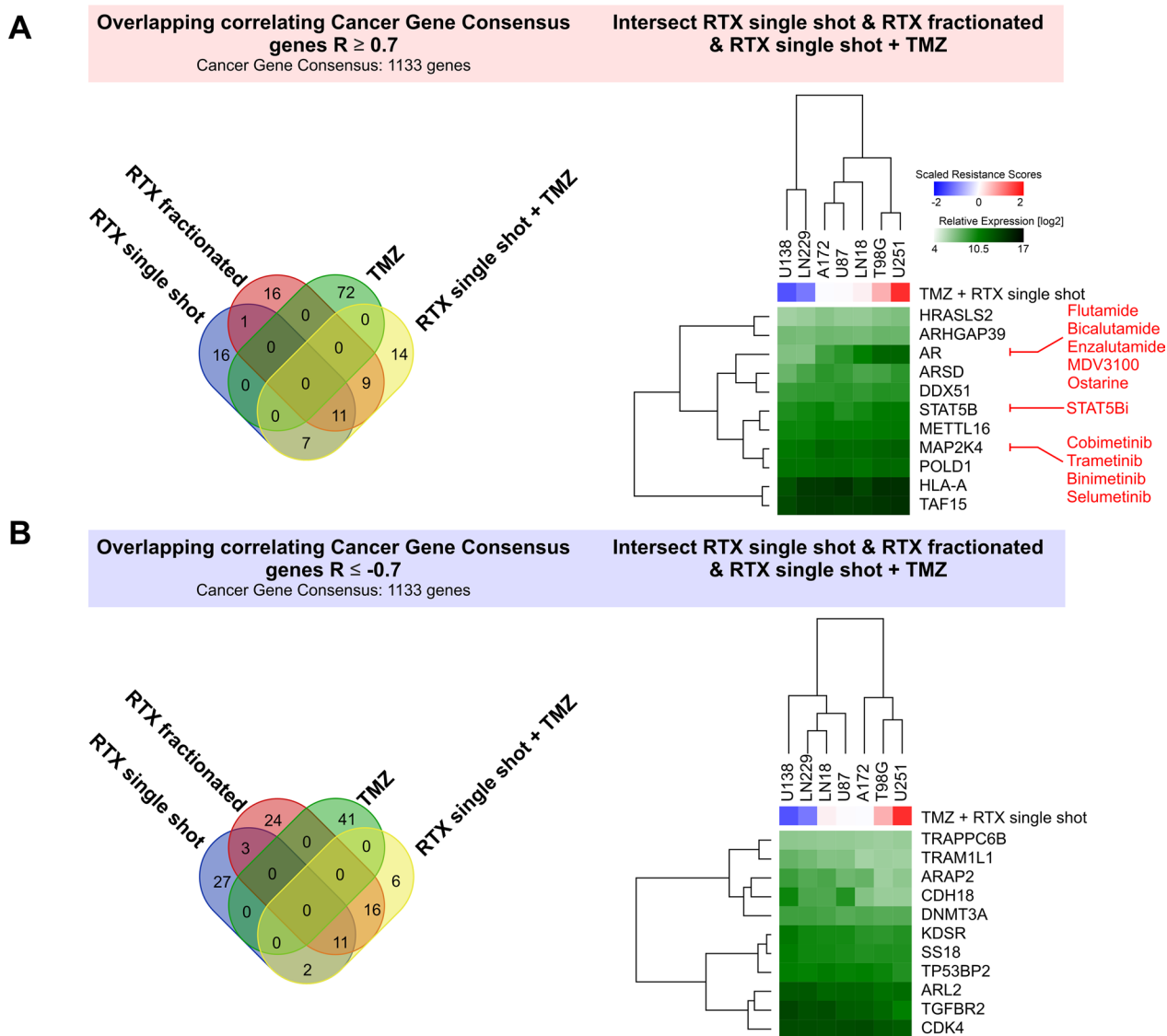


Fig. 4 Integration of mRNA expression data of cancer gene consensus (CGC) genes with inherent therapy resistance in glioblastoma cell lines. **a** Intersect analysis of CGC genes whose log₂ mRNA expression levels show significant positive ($R \geq 0.7$) correlation with inherent resistance to single-shot RTX, fractionated RTX (red), TMZ (green), and single-shot RTX + TMZ (yellow, left). Hierarchical clustering of relative log₂ mRNA expression levels of 11 intersect genes correlating with resistance to single-shot RTX, fractionated RTX, and single-shot RTX + TMZ (right). Scaled scores of resistance to single-shot RTX + TMZ are depicted, and drugs antagonizing corresponding gene products are indicated in red. **b** Overlap analysis of CGC genes whose log₂ mRNA expression shows significant negative ($R \leq -0.7$) correlation with inherent resistance to single-shot RTX, fractionated RTX, TMZ and single-shot RTX + TMZ, and hierarchical clustering of relative log₂ mRNA expression levels of 11 intersect genes

Gene set enrichment analyses (GSEAs) identify several signaling circuits as potential contributors to inherent therapy resistance in glioblastoma cells

Stepping from the single gene to the gene set level, we performed pre-ranked gene set enrichment analyses (GSEAs) on the bases of the obtained correlation coefficients (Figs. 3 and 4) and the MSigDB Hallmarks collection which contains ground-truth derived gene sets reflecting the regulation of common biological processes

[9]. With an FDR q-value cut-off of ≤ 0.1 , a total of 21 gene sets with positive enrichment were found, and 14 gene sets with negative enrichment (Fig. 5a). Gene sets that showed positive/negative enrichment for resistance against at least two of the four treatments included process categories of the core metabolism, such as GLYCOLYSIS and OXIDATIVE_PHOSPHORYLATION, development (ADIPOGENESIS), and immune mechanisms (INTERFERON_ALPHA_RESPONSE), thus

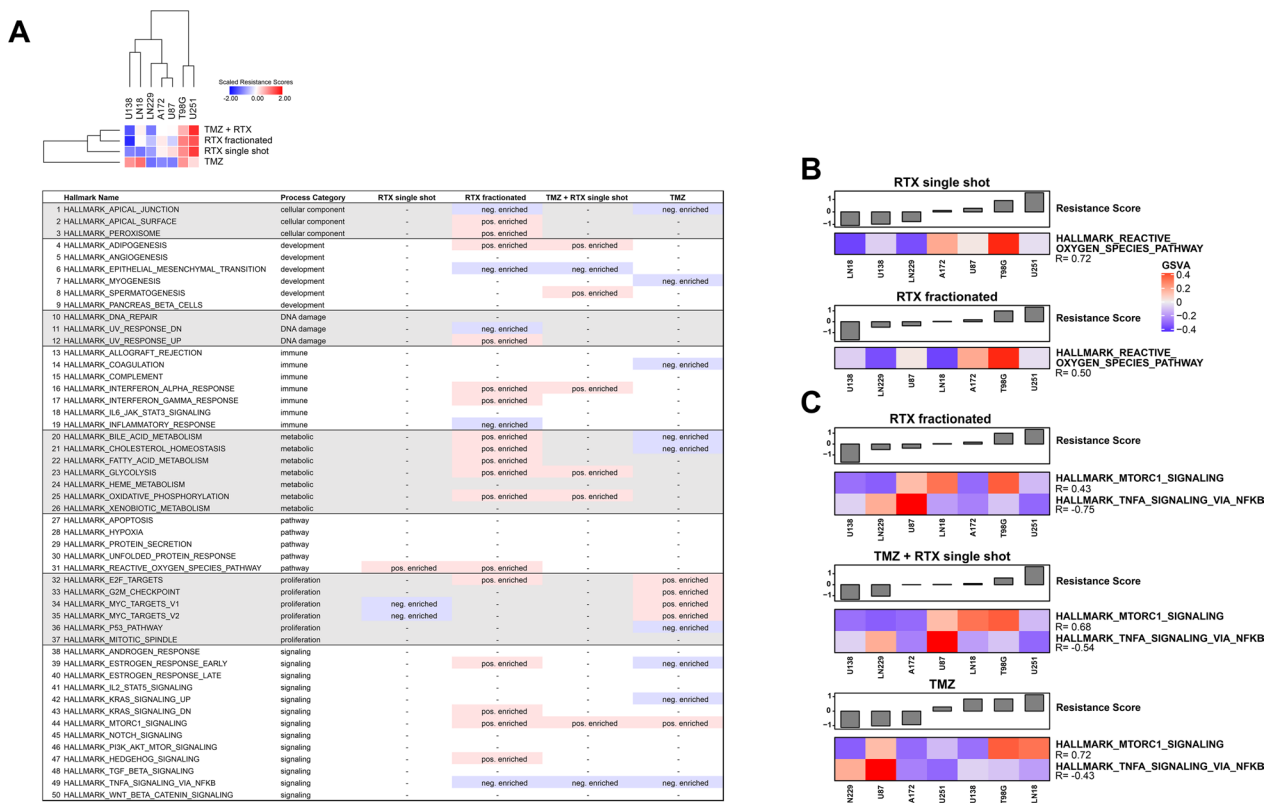


Fig. 5 Gene set enrichment analysis (GSEA) on the basis of genes correlating with therapy resistance identifies pathways of potential contribution to therapy resistance in human glioblastoma cell lines. **a** Tabular presentation of pre-ranked gene set enrichment analysis (GSEA) results on the basis of obtained correlation coefficients (therapy resistance scores vs. gene expression data), and the MSigDB hallmarks collection [9] (FDR q-value cut-off ≤ 0.1). Positively enriched hallmark gene sets are depicted in pink, and negatively enriched hallmark gene sets are depicted in blue. **b, c** Correlation analysis of gene set variation indices as determined by gene set variation analysis (GSVA), and therapy resistance scores to fractionated RTX, single-shot RTX + TMZ, and sole TMZ

according with previous reports [67–73]. Hallmark gene sets found to be negatively enriched with resistance against at least two of the four treatments included EPITHELIAL_MESENCHYMAL_TRANSITION [74, 75] and APICAL_JUNCTION [76] (Fig. 5a). For resistance against treatments comprising IR, the hallmark gene set REACTIVE_OXYGEN_SPECIES_PATHWAY was positively enriched, and the maximal intersect for enrichment with resistance against three treatments was observed for MTORC1_SIGNALING (positive), and TNFA_SIGNALING_VIA_NFKB (negative). Inverting this workflow by first reducing the dimensionality of the expression data by single-sample gene set variation analysis (GSVA), followed by correlation analyses with the obtained GSVA scores and therapy resistance scores basically confirmed these results (Fig. 5b, c).

Leading edge analyses (LEAs) of GSEA-derived gene sets identify druggable candidates and their functional interaction networks

Among the gene sets we identified to be positively or negatively enriched in therapy-resistant glioblastoma cell lines (Fig. 5a, b), we decided to concentrate on REACTIVE_OXYGEN_SPECIES_PATHWAY, MTORC1_SIGNALING and TNFA_SIGNALING_VIA_NFKB [10, 11, 77]. Leading edge analyses (LEAs) were performed by constructing functional interaction networks in Cytoscape. For REACTIVE_OXYGEN_SPECIES_PATHWAY, the leading edge genes comprised a circuit of thioredoxin/peroxiredoxin metabolism and glutathione (GSH) synthesis [78–80] (Fig. 6a and Additional file 1: Table S6) which in view of available drugs also appeared the most interesting vulnerabilities for sensitization in combined modality treatment approaches (Fig. 6b and Additional file 1: Table S6). Corresponding analyses for MTORC1_SIGNALING revealed druggable subnetworks involved in chaperoning, prolyl hydroxylation, proteasomal function, and DNA synthesis and repair, plus

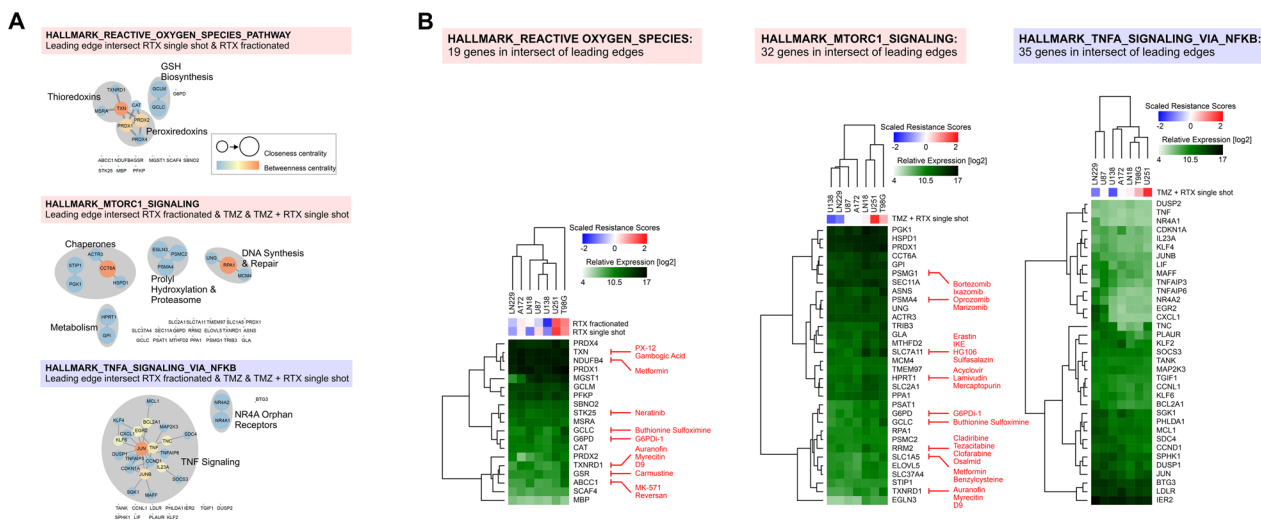


Fig. 6 Leading edge analyses (LEAs) via functional interaction networks and hierarchical clustering. **a** Functional interaction networks of the leading edge intersect genes in hallmark gene sets REACTIVE_OXYGEN_SPECIES_PATHWAY, MTORC1_SIGNALING, and TNFA_SIGNALING_VIA_NFKB as identified by GSEA in Fig. 5A. **b** Hierarchical clustering of relative log₂ mRNA expression levels of the respective leading edge intersect genes. Scaled scores of inherent therapy resistances are shown by unsupervised hierarchical clustering, and drugs antagonizing the respective gene products are indicated in red

individual genes overlapping with thioredoxin/peroxiredoxin metabolism and GSH synthesis as disclosed in the leading edge of REACTIVE_OXYGEN_SPECIES_PATHWAY and involved in ferroptosis and autophagy regulation [81, 82] (Fig. 6a, b and Additional file 1: Table S6). Finally, the leading edge of negatively enriched TNFA_SIGNALING_VIA_NFKB was mainly composed of candidates directly involved in TNF/NF-κB signaling [83, 84] (Fig. 6a, b and Additional file 1: Table S6).

Expression of candidate genes for targeted sensitization of glioblastoma as identified by GSEA and LEA is not driven by corresponding CNAs and only marginally anti-correlates with respective promotor methylation

In order to examine if expression of the leading edge genes identified by our correlation/GSEA workflow is reflected by CNAs on the DNA level or by CpG methylation, we integrated the corresponding data sets. Unexpectedly, no significant association between the transcriptome and the CNA level was observed (not

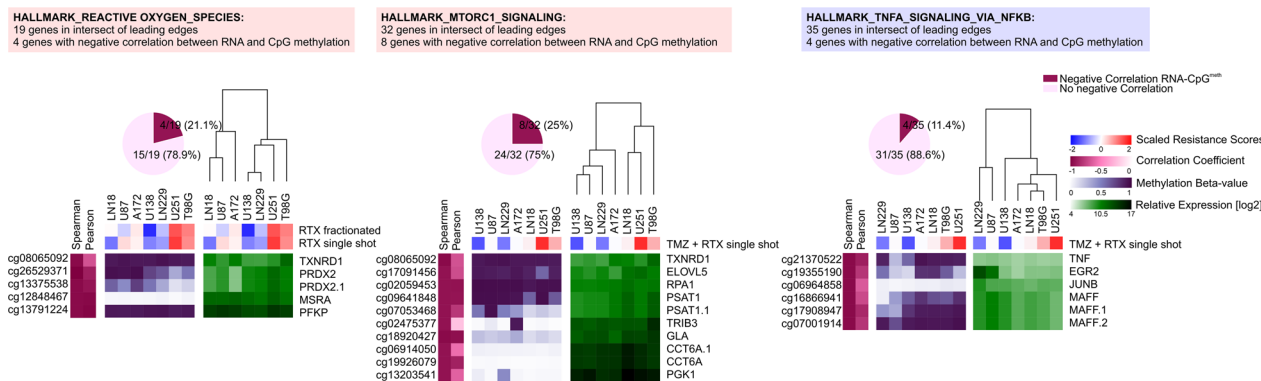


Fig. 7 CpG methylation status of leading edge intersect genes shows poor correlation between DNA methylation and therapy resistance. Correlation analyses of DNA methylation beta values (shown in purple) and relative log₂ mRNA expression levels (shown in green) of leading edge intersect genes of the REACTIVE_OXYGEN_SPECIES_PATHWAY, MTORC1_SIGNALING, and TNFA_SIGNALING_VIA_NFKB hallmark gene sets. Coefficients of significant negative correlation are depicted by heat map clustering (shown in dark pink), and scaled resistance scores to single-shot and fractionated RTX (REACTIVE_OXYGEN_SPECIES_PATHWAY), or single-shot RTX + TMZ (MTORC1_SIGNALING, and TNFA_SIGNALING_VIA_NFKB) are shown by unsupervised hierarchical clustering

shown). Furthermore, significant negative correlation with promotor methylation was only observed for a minor subset of genes (Fig. 7) suggesting that other mechanisms dominate gene expression in this context and that integrative approaches such as the one described in the present study require mRNA expression data, rather than CNA or DNA methylation data.

In summary, our data show that workflows correlating mRNA expression data with PCA-derived scores of inherent therapy resistance, followed by GSEA and LEA can reveal therapy resistance markers and potential vulnerabilities for pharmacological sensitization—both previously reported ones and hitherto unknown candidates, and thereby can open new perspectives for mechanism-based, combined modality treatment of glioblastoma and probably also of other cancer entities.

Discussion

Inherent therapy resistance is a major challenge in the treatment of various malignancies. Glioblastoma is particularly well-known for its high degree of treatment resistance, accounting for its dismal prognosis [4]. The identification of key regulators that orchestrate this resistance is therefore inevitable in order to disclose novel perspectives of targeted combined modality therapy and to improve treatment outcome [29]. We recently showed that integrating scores of inherent therapy resistance as extracted from clonogenic survival data with mRNA expression data of the DNA damage response is a suitable approach to identify new candidates for targeted sensitization of glioblastoma [7, 8]. Here, we expanded this workflow to global mRNA expression data and additional molecular levels, including DNA methylome and chromosomal CNAs—all collected under treatment-naïve conditions which most closely resemble the clinical situation of tissue sampling in form of tumor biopsies and resections. In accordance with our preceding study, the identification of O⁶-methylguanine-DNA-methyltransferase (MGMT) as the best correlating candidate among all genes with positive correlation of mRNA expression with resistance to TMZ provided a proof-of-concept for the feasibility of our approach. Furthermore, on the single gene level, we identified the androgen receptor (AR) as a crucial positive correlator with inherent resistance to three of the four types of treatment—a candidate which is already successfully therapeutically addressed in several cancer entities, such as prostate cancer [58, 61, 85], and thus is eligible to rapid evaluation in glioblastoma [52]. Another gene whose expression level correlated positively with resistance to three types of glioblastoma treatment was mitogen-activated protein kinase kinase

4 (MAP2K4) [63]. Various inhibitors of the MAP kinase family have been developed and several of them, including trametinib and cobimetinib, are readily approved for clinical use in other cancer entities [86]. However, it is known that these compounds commonly do not pass the blood brain barrier (BBB) which for instance undermines efficient treatment of brain metastases originating from MAP kinase-driven melanoma [87, 88]. Therefore, new BBB-passing MAP kinase inhibitors such as E6201 are currently in development [89–92]. Our data suggest that these inhibitors may be interesting candidates for targeted sensitization of glioblastoma to IR and/or TMZ.

In order to identify gene sets, networks, and signaling circuits rather than single genes, we made use of pre-ranked gene set analyses (GSEAs) on the basis of the correlation coefficients (gene expression vs. therapy resistance) followed by leading edge analyses (LEAs). This indeed yielded several candidates whose pharmacological targeting appears interesting in the context of targeted radio- and/or chemosensitization of glioblastoma and—more importantly—for which refined drugs are readily available. Among these were the MSigDB hallmark gene sets REACTIVE_OXYGEN_SPECIES_PATHWAY and MTORC1_SIGNALING, both of which comprise candidates that can be well-targeted by various available drugs [93, 94]. Mechanistically, the identified regulatory circuits have major implications for death and/or survival pathways, such as ferroptosis and autophagy [81, 95], and crucial pro-survival players would represent interesting targets in order to break glioblastoma cell death evasion and resistance against IR [96–98] or TMZ [99], respectively.

When tracing the mRNA expression data back to the chromosomal CNA status, we did not observe relevant associations. Furthermore, CpG methylation status did only in part reflect the obtained mRNA expression data. Accordingly, other mechanisms, including posttranscriptional regulation of mRNA expression by microRNAs (miRNAs) [100], may be involved in glioblastoma gene regulation accounting for the observed therapy resistance-associated mRNA expression patterns, and this would also fit with several recent reports identifying miRNA signatures as outcome prognosticators of glioblastoma [101–104]. It is in accordance with previous reports which found only marginal associations between the methylation status of MGMT promotor and mRNA or protein expression levels in glioblastoma patients [49, 105]. Hence, it is feasible to assume that our integrative approach requires mRNA expression data, rather than DNA methylation or CNA data to obtain robust results. In how far (phospho-)proteomic data would further improve the study outcome remains to be investigated [106].

Similar systematic in vitro analyses of therapy resistance on the basis of clonogenic survival data and multi-level molecular data are rare [107, 108], not only in glioblastoma [109–111]. Most studies of similar purpose integrate molecular data from patient material provided by publicly available databases such as TCGA with clinical data in order to identify genes with association to therapy resistance [22, 112–114]. However, the molecular data obtained from such cohorts are often of high complexity given that biopsied/resected patient material usually comprises complex tumor tissue, including tumor stroma and normal tissue cells rather than only tumor cells [115, 116]. Furthermore, information on treatment courses and clinical endpoints commonly is scarce and/or incomplete, thus further hampering the interpretability of these data. Our results do not only provide proof-of-concept for the feasibility of the chosen integrative in vitro approach. The data sets generated in the present study comprising functional (clonogenic survival data) and multi-level molecular data (mRNA transcriptome, DNA methylome, chromosomal CNA, and SKY FISH) of very commonly used glioblastoma cell lines (in an unperurbed, untreated stage) also represent a valuable toolbox which can be readily interrogated by other researchers in the field of glioblastoma therapy resistance. Nevertheless, since dynamic changes on the analyzed molecular levels (particularly on the transcriptome and on the methylome level) are to be expected in response to therapy and may well be causative for the emergence of acquired therapy resistance [30, 117–119], further research is certainly needed. Finally, the integrative nature of the described workflow can be adapted to other disease models, such as 3D cell culture and organoids [120], since this may impact both, global mRNA expression and therapy resistance [121–123].

Abbreviations

A4GALT	Lactosylceramide 4-alpha-galactosyltransferase
ABC	ATP binding cassette
ABCC1	ATP binding cassette subfamily C member 1
aCGH	Array comparative genomic hybridization
ACTR3	Actin related protein 3
AKT	V-Akt murine thymoma viral oncogene
AKT1	V-Akt murine thymoma viral oncogene 1
ANSI	American National Standards Institute
AP2	Adaptor related protein complex 2
AP2B1	Adaptor related protein complex 2 subunit beta 1
AR	Androgen receptor
ARAP2	ArfGAP with RhoGAP domain, ankyrin repeat and PH Domain 2
ARHGAP39	Rho GTPase activating protein 39
ARL2	ADP ribosylation factor like GTPase 2
ARSD	Arylsulfatase D
ASCT2	Alanine serine cysteine transporter 2
ASNS	Asparagine synthetase
ATCC	American Type Culture Collection
BBB	Blood brain barrier
BCL2A1	BCL2 related protein A1
BCR	BTB-Cul3-Rbx1

BTB	BR-C, Ttk and bab
BTG3	BTG anti-proliferation factor 3
CASP1	Caspase-1
CAT	Catalase
C1GALT1	Core 1 glycoprotein-N-acetyl-galactosamine-3-beta-galactosyltransferase 1
CCND1	Cyclin D1
CCNL1	Cyclin L1
CCT6A	Chaperonin containing TCP1 subunit 6A
CDH18	Cadherin 18
CDK4	Cyclin dependent kinase 4
CDKN1A	Cyclin dependent kinase inhibitor 1A
CDS1	Phosphatidate cytidylyltransferase 1
CFH	Complement factor H
CGC	Cancer gene consensus
CH13L1	Chitinase-3-like protein 1
CIMP	CpG island methylator phenotype
CIN	Chromosomal instability
CNA	Copy number alteration
COSMIC	Catalogue of somatic mutations in cancer
CSF1	Colony stimulating factor 1
CUL3	Cullin 3
CXCL1	C-X-C motif chemokine ligand 1
CXCR4	C-X-C motif chemokine receptor 4
D-MEM	Dulbecco's modified eagle medium
DAPI	4',6-Diamidino-2-phenylindole
DDR	DNA damage response
DDX51	DEAD-box helicase 51
DNMT3A	DNA methyltransferase 3 alpha
DUSP1	Dual specificity phosphatase 1
DUSP2	Dual specificity phosphatase 2
EGFR	Epidermal growth factor receptor
EGLN3	Egl-9 family hypoxia inducible factor 3
EGFRVIII	Epidermal growth factor receptor variant III
EGR2	Early growth response 2
ELOVL5	Fatty acid elongase 5
EMT	Epithelial-mesenchymal transition
ERK	Extracellular signal-regulated kinase
FCS	Fetal calf serum
FDR	False recovery rate
FIR	Fractionated IR
FOXP3	Forkhead box protein 3
G6PD	Glucose-6-phosphate dehydrogenase
GCKIII	Germinal centre kinase III
GCLC	Glutamate-cysteine ligase catalytic subunit
GCLM	Glutamate-cysteine ligase modifier subunit
GEO	Gene expression omnibus
GLA	Galactosidase alpha
GPI	Glucose-6-phosphate isomerase
GSC	Glioma stem cell
GSEA	Gene set enrichment analysis
GSH	Glutathione
GSR	Glutathione-disulfide reductase
GSSG	Glutathione disulfide
GSPA	Gene set variation analysis
HLA-A	Major histocompatibility complex, class I, A
HPRT1	Hypoxanthine phosphoribosyltransferase 1
HRASL52	HRAS-like suppressor 2
HSPD1	Heat shock protein family D member 1
HAP1	Huntingtin-associated protein 1
HTT	Huntingtin
IDO1	Indoleamine 2,3-dioxygenase 1
IER2	Immediate early response gene 2
IL2	Interleukin 2
IL2RA	Interleukin-2 receptor alpha
IL4	Interleukin 4
IL23A	Interleukin 23 subunit alpha
IR	Ionizing radiation
ISCN	International system for cytogenetic nomenclature
JAK	Janus kinase

JNK	C-Jun N-terminal kinase	RAS	Rat sarcoma
JUN	Jun proto-oncogene	RBX1	Ring box 1
JUNB	Jun B proto-oncogene	RELB	Transcription factor RelB
KDSR	3-Ketodihydroshingosine reductase	RING	Really interesting new gene
KEAP1	Kelch like ECH associated protein 1	RNAseq	RNA sequencing
KLF2	Kruppel like factor 2	ROS	Reactive oxygen species
KLF4	Kruppel like factor 4	RPA1	Replication protein A1
KLF6	Kruppel like factor 6	rRNA	Ribosomal RNA
KLHL11	Kelch-like family member 11	RRM2	Ribonucleotide reductase regulatory subunit M2
KLK2	Kallikrein related peptidase 2	RTX	Radiotherapy
KLK3	Kallikrein related peptidase 3	SAP	Stress-activated protein
LDLR	Low density lipoprotein receptor	SBNO2	Strawberry Notch homolog 2
LEA	Leading edge analysis	SCAF4	SR-related CTD associated factor 4
LGG	Low-grade glioma	SDC4	Syndecan 4
LIF	Interleukin 6 family cytokine	SEC11A	SEC11 homolog A
LKB1	Liver kinase B1	SGK1	Serum/glucocorticoid regulated kinase 1
MAFF	MAF BZIP transcription factor F	SKY FISH	Spectral karyotyping fluorescent in situ hybridization
MAP	Mitogen-activated protein kinase	SLC1A5	Solute carrier family 1 member 5
MAP2K3	Mitogen-activated protein kinase kinase 3	SLC2A1	Solute carrier family 2 member 1
MAP2K4	Mitogen-activated protein kinase kinase 4	SLC7A11	Solute carrier family 7 member 11
MAPK	Mitogen-activated protein kinase	SLC25A11	Solute carrier family 25 member 11
MBP	Myelin basic protein	SLC37A4	Solute carrier family 37 member 4
MC	Mediator complex	SMO	Smoothened
MCL1	Induced myeloid leukemia cell differentiation protein Mcl-1	SNP	Single nucleotide polymorphism
MCM4	Minichromosome maintenance complex component 4	SOCS3	Suppressor of cytokine signaling 3
MCM15	Mediator complex subunit 15	SOD1	Superoxide dismutase 1
METTL16	Methyltransferase 16	SOX	Sry-type HMG box
MGMT	O ⁶ -methylguanine-DNA-methyltransferase	SOX2	Sry-type HMG box 2
MGST1	Microsomal glutathione S-transferase 1	SOX10	Sry-type HMG box 10
miRNA	MicroRNA	SPHK1	Sphingosine kinase 1
MSRA	Methionine sulfoxide reductase A	SS18	SS18 subunit of BAF chromatin remodeling complex
MTHFD2	Methylene-tetrahydrofolate dehydrogenase 2	ssGSEA	Single-sample GSEA
mTORC1	Mammalian target of rapamycin complex 1	SSIR	Single-shot IR
MYNN	Myoneurin	STAT	Signal transducer and activator of transcription
NDUFB4	NADH-ubiquinone oxidoreductase subunit B4	STAT5B	Signal transducer and activator of transcription 5B
NES	Nestin	STIP1	Stress induced phosphoprotein 1
NF-κB	Nuclear factor κB	STK25	Serine/threonine kinase 25
NF1	Neurofibromin	STR	Short tandem repeat
NOTCH3	Notch receptor 3	SYPL1	Synaptophysin-like 1
NPEPPS	Puromycin-sensitive aminopeptidase M1	SYPL2	Synaptophysin-like 2
NR4A1	Nuclear receptor subfamily 4 group A member 1	SYT14	Synaptotagmin-14
NR4A2	Nuclear receptor subfamily 4 group A member 2	TAF15	TATA-box binding protein associated factor 15
NRF2	NF-2-related factor 2	TANK	TRAF family member associated NF-κB activator
NSCLC	Non-small cell lung cancer	TGFBR1	Transforming growth factor beta receptor 1
PBS	Phosphate-buffered saline	TGFBR2	Transforming growth factor beta receptor 2
PCA	Principal component analysis	TGIF1	TGFβ induced factor homeobox 1
PDGFR	Platelet-derived growth factor receptor	TMEM97	Transmembrane protein 97
PDGFRA	Platelet-derived growth factor receptor alpha	TMZ	Temozolomide
PFKP	Phosphofructokinase, platelet	TNC	Tenascin C
PGK1	Phosphoglycerate kinase 1	TNF	Tumor necrosis factor
PHLDA1	Pleckstrin homology like domain family A member 1	TNFA	Tumor necrosis factor alpha
PI3K	Phosphatidylinositol 3-kinase	TNFAIP3	Tumor necrosis factor alpha induced protein 3
PLAAT2	Phospholipase A and acyltransferase 2	TNFAIP6	Tumor necrosis factor alpha induced protein 6
PLAUR	Plasminogen activator, urokinase receptor	TNFRSF1A	Tumor necrosis factor receptor super family member 1A
POL1	RNA polymerase 1	TP53BP2	Tumor protein p53 binding protein 2
POLA1	DNA polymerase alpha 1, catalytic subunit	TRADD	TNFRSF1A associated via death domain
POLD1	DNA polymerase delta 1, catalytic subunit	TRAM1L1	Translocation associated membrane protein 1 like 1
POLR1F	RNA polymerase 1 subunit F	TRAPP6B	Trafficking protein particle complex, subunit 6B
PPA1	Inorganic pyrophosphatase 1	TRIB3	Tribbles pseudokinase 3
PRDX1	Peroxiredoxin 1	TRX	Thioredoxin
PRDX2	Peroxiredoxin 2	TSNAXIP1	Translin-associated X-interacting protein 1
PRDX4	Peroxiredoxin 4	TWISTNB	TWIST neighbor
PRL	Prolactin	TXN	Thioredoxin
PSAT1	Phosphoserine aminotransferase 1	TXNDC17	Thioredoxin domain containing protein 17
PSMA4	Proteasomal 20S subunit alpha 4	TXNRD1	Thioredoxin reductase 1
PSMB3	Proteasomal subunit beta 3	UNG	Uracil DNA glycosylase
PSMC2	Proteasome 26S subunit, ATPase 2	WNT	Wingless and Int-1
PSMG1	Proteasome assembly chaperone 1	ZDHHC17	Zinc finger DHHC-type palmitoyltransferase 17
PSMG2	Proteasome assembly chaperone 2	ZZEF1	ZZ-type zinc finger and EF-hand domain-containing protein 1
PSMG4	Proteasome assembly chaperone 4		

Supplementary Information

The online version contains supplementary material available at <https://doi.org/10.1186/s13014-023-02241-4>.

Additional file 1. Supplementary tables.

Additional file 2. Compilation of all molecular data collected in this study.

Acknowledgements

We thank Janina Mielke, Michael Rüter, Isabella Zagorski, Laura Holler, and Steffen Heuer for technical assistance.

Author contributions

LES, DP, PW, NB, DFF, AEN, MS, TH, JH, MN, CB, HZ, KL, KU, and MO conceived the experiments, analyzed the data, and discussed the data. LES, DP, PW, NB, DFF, AEN, MS, TH, JH, KU and MO performed the experiments. LES, KU, and KL prepared the figures, and performed bioinformatical and statistical analyses. MO, LES, KU, and KL wrote the manuscript. All the authors read and approved the final manuscript.

Funding

Open Access funding enabled and organized by Projekt DEAL. This work was funded by the FoEfoLe program of the Medical Faculty of the *Ludwig-Maximilians-Universität* (LMU) Munich, the *Deutsche Forschungsgemeinschaft* (INST 409/126–1 FUGG, INST 409/20–1 FUGG, and INST 409/22–1 FUGG), and the *Bundesministerium für Bildung und Forschung* (German Cancer Consortium (DKTK), 02NUK047C BMBF ZISstrans, and 02NUK061C BMBF METABOLIST).

Availability of data and materials

The gene expression data and the array CGH data presented in this study are publicly available at Gene Expression Omnibus (GEO) under the super set accession number: GSE119637. For the review process, reviewers can access the data under the link <https://www.ncbi.nlm.nih.gov/geo/query/acc.cgi?acc=GSE119637> using the token 'sqnocumrvofmrv'.

Declarations

Ethics approval and consent to participate

Not applicable.

Consent for publication

Not applicable.

Competing interests

All authors declare that there is no conflict of interest.

Author details

¹Department of Radiation Oncology, University Hospital, LMU München, Marchioninistrasse 15, 81377 Munich, Germany. ²Research Unit Radiation Cytogenetics (Zyto), Helmholtz Center Munich, German Research Center for Environmental Health GmbH, 85764 Neuherberg, Germany. ³Clinical Cooperation Group 'Personalized Radiotherapy in Head and Neck Cancer' Helmholtz Center Munich, German Research Center for Environmental Health GmbH, Neuherberg, Germany. ⁴German Cancer Consortium (DKTK), Munich, Germany. ⁵German Cancer Research Center (DKFZ), Heidelberg, Germany. ⁶Bavarian Cancer Research Center (BKFZ), Munich, Germany.

Received: 7 February 2023 Accepted: 6 March 2023

Published online: 11 March 2023

References

- Fisher JL, et al. Epidemiology of brain tumors. *Neurol Clin.* 2007;25(4):867–90.
- Barani IJ, Larson DA. Radiation therapy of glioblastoma. *Cancer Treat Res.* 2015;163:49–73.
- Stupp R, et al. Radiotherapy plus concomitant and adjuvant temozolomide for glioblastoma. *N Engl J Med.* 2005;352(10):987–96.
- Osuka S, Van Meir EG. Overcoming therapeutic resistance in glioblastoma: the way forward. *J Clin Invest.* 2017;127(2):415–26.
- Veliz I, et al. Advances and challenges in the molecular biology and treatment of glioblastoma—is there any hope for the future? *Ann Transl Med.* 2015;3(1):7.
- Degorre C, et al. Bench to bedside radiosensitizer development strategy for newly diagnosed glioblastoma. *Radiat Oncol.* 2021;16(1):191.
- Schnöller LE, et al. Integrative analysis of therapy resistance and transcriptomic profiling data in glioblastoma cells identifies sensitization vulnerabilities for combined modality radiochemotherapy. *Radiat Oncol.* 2022;17(1):79.
- Unkel S, Belka C, Lauber K. On the analysis of clonogenic survival data: Statistical alternatives to the linear-quadratic model. *Radiat Oncol.* 2016;11:11.
- Subramanian A, et al. Gene set enrichment analysis: a knowledge-based approach for interpreting genome-wide expression profiles. *Proc Natl Acad Sci U S A.* 2005;102(43):15545–50.
- Hoeffler CA, Klann E. mTOR signaling: at the crossroads of plasticity, memory and disease. *Trends Neurosci.* 2010;33(2):67–75.
- Nogueira V, Hay N. Molecular pathways: reactive oxygen species homeostasis in cancer cells and implications for cancer therapy. *Clin Cancer Res.* 2013;19(16):4309–14.
- Allen M, et al. Origin of the U87MG glioma cell line: Good news and bad news. *Sci Transl Med.* 2016;8(354):354re3.
- ANSI/ATCC ASN-0002–2011. Authentication of Human Cell Lines Standardization of STR Profiling. ANSI eStandards Store, 2012.pdf.
- Brix N, et al. Analysis of clonogenic growth in vitro. *Nat Protoc.* 2021;16(11):4963–91.
- Braselmann H, et al. SKY and FISH analysis of radiation-induced chromosome aberrations: a comparison of whole and partial genome analysis. *Mutat Res.* 2005;578(1–2):124–33.
- Shaffer LG, McGowan-Jordan J, Schmid M. ISCN 2013: an international system for human cytogenetic nomenclature. Karger Medical and Scientific Publishers. 2013
- Michna A, et al. Transcriptomic analyses of the radiation response in head and neck squamous cell carcinoma subclones with different radiation sensitivity: time-course gene expression profiles and gene association networks. *Radiat Oncol.* 2016;11:94.
- Wilke CM, et al. A genomic copy number signature predicts radiation exposure in post-Chernobyl breast cancer. *Int J Cancer.* 2018;143(6):1505–15.
- Hess J, et al. Gain of chromosome band 7q11 in papillary thyroid carcinomas of young patients is associated with exposure to low-dose irradiation. *Proc Natl Acad Sci U S A.* 2011;108(23):9595–600.
- Aryee MJ, et al. Minfi: a flexible and comprehensive Bioconductor package for the analysis of Infinium DNA methylation microarrays. *Bioinformatics.* 2014;30(10):1363–9.
- Ceccarelli M, et al. Molecular profiling reveals biologically discrete subsets and pathways of progression in diffuse glioma. *Cell.* 2016;164(3):550–63.
- Cancer Genome Atlas Research, N. Comprehensive genomic characterization defines human glioblastoma genes and core pathways. *Nature.* 2008;455(7216):1061–8.
- Wang Q, et al. Tumor evolution of glioma-intrinsic gene expression subtypes associates with immunological changes in the microenvironment. *Cancer Cell.* 2017;32(1):42 e6–56 e6.
- Verhaak RG, et al. Integrated genomic analysis identifies clinically relevant subtypes of glioblastoma characterized by abnormalities in PDGFRA, IDH1, EGFR, and NF1. *Cancer Cell.* 2010;17(1):98–110.
- Sondka Z, et al. The COSMIC Cancer Gene Census: describing genetic dysfunction across all human cancers. *Nat Rev Cancer.* 2018;18(11):696–705.
- Hanzelmann S, Castelo R, Guinney J. GSEA: gene set variation analysis for microarray and RNA-seq data. *BMC Bioinformatics.* 2013;14:7.
- Corso CD, Bindra RS. Success and failures of combined modalities in glioblastoma multiforme: old problems and new directions. *Semin Radiat Oncol.* 2016;26(4):281–98.
- Shirazi HA, et al. Combined modality approaches in the management of adult glioblastoma. *Front Oncol.* 2011;1:36.

29. Zhang P, et al. Current opinion on molecular characterization for GBM classification in guiding clinical diagnosis, prognosis, and therapy. *Front Mol Biosci.* 2020;7: 562798.
30. Bhat KPL, et al. Mesenchymal differentiation mediated by NF-kappaB promotes radiation resistance in glioblastoma. *Cancer Cell.* 2013;24(3):331–46.
31. Huang M, et al. Wnt-mediated endothelial transformation into mesenchymal stem cell-like cells induces chemoresistance in glioblastoma. *Sci Transl Med.* 2020;12(532):eaay7522.
32. Piao Y, et al. Acquired resistance to anti-VEGF therapy in glioblastoma is associated with a mesenchymal transition. *Clin Cancer Res.* 2013;19(16):4392–403.
33. Park AK, et al. Subtype-specific signaling pathways and genomic aberrations associated with prognosis of glioblastoma. *Neuro Oncol.* 2019;21(1):59–70.
34. Tjihuis AE, Johnson SC, McClelland SE. The emerging links between chromosomal instability (CIN), metastasis, inflammation and tumour immunity. *Mol Cytogenet.* 2019;12:17.
35. van Dijk E, et al. Chromosomal copy number heterogeneity predicts survival rates across cancers. *Nat Commun.* 2021;12(1):3188.
36. Sansregret L, Vanhaesebroeck B, Swanton C. Determinants and clinical implications of chromosomal instability in cancer. *Nat Rev Clin Oncol.* 2018;15(3):139–50.
37. Bakhoun SF, Cantley LC. The multifaceted role of chromosomal instability in cancer and its microenvironment. *Cell.* 2018;174(6):1347–60.
38. Godek KM, et al. Chromosomal instability affects the tumorigenicity of glioblastoma tumor-initiating cells. *Cancer Discov.* 2016;6(5):532–45.
39. Balzano E, et al. Characterization of chromosomal instability in glioblastoma. *Front Genet.* 2021;12: 810793.
40. Bagci O, Kurtgoz S. Amplification of cellular oncogenes in solid tumors. *N Am J Med Sci.* 2015;7(8):341–6.
41. Schwab M. Amplification of oncogenes in human cancer cells. *BioEssays.* 1998;20(6):473–9.
42. Phillips HS, et al. Molecular subclasses of high-grade glioma predict prognosis, delineate a pattern of disease progression, and resemble stages in neurogenesis. *Cancer Cell.* 2006;9(3):157–73.
43. Behnan J, Finocchiaro G, Hanna G. The landscape of the mesenchymal signature in brain tumours. *Brain.* 2019;142(4):847–66.
44. Kupp R, et al. Lineage-restricted OLIG2-RTK signaling governs the molecular subtype of glioma stem-like cells. *Cell Rep.* 2016;16(11):2838–45.
45. Guo M, et al. SFRP2 induces a mesenchymal subtype transition by suppression of SOX2 in glioblastoma. *Oncogene.* 2021;40(32):5066–80.
46. Muraguchi T, et al. NKX22 suppresses self-renewal of glioma-initiating cells. *Cancer Res.* 2011;71(3):1135–45.
47. Brennan CW, et al. The somatic genomic landscape of glioblastoma. *Cell.* 2013;155(2):462–77.
48. Hegi ME, et al. MGMT gene silencing and benefit from temozolomide in glioblastoma. *N Engl J Med.* 2005;352(10):997–1003.
49. Yu W, et al. O(6)-Methylguanine-DNA methyltransferase (MGMT): challenges and new opportunities in glioma chemotherapy. *Front Oncol.* 2019;9:1547.
50. Dallavalle S, et al. Antitumor activity of novel POLA1-HDAC11 dual inhibitors. *Eur J Med Chem.* 2022;228: 113971.
51. Hu C, et al. The androgen receptor expression and association with patient's survival in different cancers. *Genomics.* 2020;112(2):1926–40.
52. Zalcman N, et al. Androgen receptor: a potential therapeutic target for glioblastoma. *Oncotarget.* 2018;9(28):19980–93.
53. Farina-Jeronimo H, et al. Androgen receptor activity is associated with worse survival in glioblastoma. *J Integr Neurosci.* 2022;21(3):86.
54. Lysiak M, et al. The sex-dependent role of the androgen receptor in glioblastoma: results of molecular analyses. *Mol Oncol.* 2022;16(19):3436–51.
55. Yu X, et al. Androgen receptor signaling regulates growth of glioblastoma multiforme in men. *Tumour Biol.* 2015;36(2):967–72.
56. Werner CK, et al. Expression of the androgen receptor governs radiation resistance in a subset of glioblastomas vulnerable to antiandrogen therapy. *Mol Cancer Ther.* 2020;19(10):2163–74.
57. Zhao N, et al. Androgen receptor, although not a specific marker for, is a novel target to suppress glioma stem cells as a therapeutic strategy for glioblastoma. *Front Oncol.* 2021;11: 616625.
58. Heinlein CA, Chang C. Androgen receptor in prostate cancer. *Endocr Rev.* 2004;25(2):276–308.
59. Giovannelli P, et al. The androgen receptor in breast cancer. *Front Endocrinol (Lausanne).* 2018;9:492.
60. Fujii S, Kagechika H. Androgen receptor modulators: a review of recent patents and reports (2012–2018). *Expert Opin Ther Pat.* 2019;29(6):439–53.
61. Kim TJ, Lee YH, Koo KC. Current status and future perspectives of androgen receptor inhibition therapy for prostate cancer: a comprehensive review. *Biomolecules.* 2021;11(4):492.
62. Palmieri C, et al. Efficacy of enobosarm, a selective androgen receptor (AR) targeting agent, correlates with the degree of AR positivity in advanced AR+/estrogen receptor (ER)+ breast cancer in an international phase 2 clinical study. *J Clin Oncol.* 2021;39(15_suppl):1020–1020.
63. Whitmarsh AJ, Davis RJ. Role of mitogen-activated protein kinase kinase 4 in cancer. *Oncogene.* 2007;26(22):3172–84.
64. Zalcman N, et al. Enough EGFR-A potential therapeutic target. *Int J Mol Sci.* 2021;22(20):10954.
65. Loh CY, et al. Signal transducer and activator of transcription (STATs) proteins in cancer and inflammation: functions and therapeutic implication. *Front Oncol.* 2019;9:48.
66. Levy DE, Darnell JE Jr. Stats: transcriptional control and biological impact. *Nat Rev Mol Cell Biol.* 2002;3(9):651–62.
67. McKelvey KJ, et al. Glycolysis and fatty acid oxidation inhibition improves survival in glioblastoma. *Front Oncol.* 2021;11: 633210.
68. Wu Z, Ho WS, Lu R. Targeting mitochondrial oxidative phosphorylation in glioblastoma therapy. *Neuromolecular Med.* 2022;24(1):18–22.
69. Stanke KM, Wilson C, Kidambi S. High expression of glycolytic genes in clinical glioblastoma patients correlates with lower survival. *Front Mol Biosci.* 2021;8: 752404.
70. Duraj T, et al. Beyond the warburg effect: oxidative and glycolytic phenotypes coexist within the metabolic heterogeneity of glioblastoma. *Cells.* 2021;10(2):202.
71. Shi Y, et al. Gboxin is an oxidative phosphorylation inhibitor that targets glioblastoma. *Nature.* 2019;567(7748):341–6.
72. Kant S, et al. Enhanced fatty acid oxidation provides glioblastoma cells metabolic plasticity to accommodate to its dynamic nutrient microenvironment. *Cell Death Dis.* 2020;11(4):253.
73. Silginer M, et al. Autocrine activation of the IFN signaling pathway may promote immune escape in glioblastoma. *Neuro Oncol.* 2017;19(10):1338–49.
74. Kalluri R, Weinberg RA. The basics of epithelial-mesenchymal transition. *J Clin Invest.* 2009;119(6):1420–8.
75. Lamouille S, Xu J, Derynck R. Molecular mechanisms of epithelial-mesenchymal transition. *Nat Rev Mol Cell Biol.* 2014;15(3):178–96.
76. Wang Q, Margolis B. Apical junctional complexes and cell polarity. *Kidney Int.* 2007;72(12):1448–58.
77. Hayden MS, Ghosh S. Regulation of NF-kappaB by TNF family cytokines. *Semin Immunol.* 2014;26(3):253–66.
78. Lee S, Kim SM, Lee RT. Thioredoxin and thioredoxin target proteins: from molecular mechanisms to functional significance. *Antioxid Redox Signal.* 2013;18(10):1165–207.
79. Lu SC. Glutathione synthesis. *Biochim Biophys Acta.* 2013;1830(5):3143–53.
80. Perkins A, et al. Peroxiredoxins: guardians against oxidative stress and modulators of peroxide signaling. *Trends Biochem Sci.* 2015;40(8):435–45.
81. Jiang X, Stockwell BR, Conrad M. Ferroptosis: mechanisms, biology and role in disease. *Nat Rev Mol Cell Biol.* 2021;22(4):266–82.
82. Dikic I, Elazar Z. Mechanism and medical implications of mammalian autophagy. *Nat Rev Mol Cell Biol.* 2018;19(6):349–64.
83. Holbrook J, et al. Tumour necrosis factor signalling in health and disease. *F1000Res.* 2019;8.
84. Aggarwal BB. Signalling pathways of the TNF superfamily: a double-edged sword. *Nat Rev Immunol.* 2003;3(9):745–56.
85. Wong YN, et al. Evolution of androgen receptor targeted therapy for advanced prostate cancer. *Nat Rev Clin Oncol.* 2014;11(6):365–76.
86. Braicu C, et al. A comprehensive review on MAPK: a promising therapeutic target in cancer. *Cancers (Basel).* 2019;11(10):1618.
87. Spagnolo F, et al. Survival of patients with metastatic melanoma and brain metastases in the era of MAP-kinase inhibitors and

- immunologic checkpoint blockade antibodies: a systematic review. *Cancer Treat Rev.* 2016;45:38–45.
88. Sullivan RJ, Flaherty K. MAP kinase signaling and inhibition in melanoma. *Oncogene.* 2013;32(19):2373–9.
 89. Gampa G, et al. Brain distribution of a novel MEK Inhibitor E6201: implications in the treatment of melanoma brain metastases. *Drug Metab Dispos.* 2018;46(5):658–66.
 90. Babiker HM, et al. E6201, an intravenous MEK1 inhibitor, achieves an exceptional response in BRAF V600E-mutated metastatic malignant melanoma with brain metastases. *Invest New Drugs.* 2019;37(4):636–45.
 91. Tibes R, et al. Safety, pharmacokinetics, and preliminary efficacy of E6201 in patients with advanced solid tumours, including melanoma: results of a phase 1 study. *Br J Cancer.* 2018;118(12):1580–5.
 92. Narita Y, et al. Novel ATP-competitive MEK inhibitor E6201 is effective against vemurafenib-resistant melanoma harboring the MEK1-C121S mutation in a preclinical model. *Mol Cancer Ther.* 2014;13(4):823–32.
 93. Perillo B, et al. ROS in cancer therapy: the bright side of the moon. *Exp Mol Med.* 2020;52(2):192–203.
 94. Zou Z, et al. mTOR signaling pathway and mTOR inhibitors in cancer: progress and challenges. *Cell Biosci.* 2020;10:31.
 95. Aman Y, et al. Autophagy in healthy aging and disease. *Nat Aging.* 2021;1(8):634–50.
 96. Tam SY, Wu VW, Law HK. Influence of autophagy on the efficacy of radiotherapy. *Radiat Oncol.* 2017;12(1):57.
 97. Galluzzi L, et al. Activating autophagy to potentiate immunogenic chemotherapy and radiation therapy. *Nat Rev Clin Oncol.* 2017;14(4):247–58.
 98. Li L, et al. The role of autophagy in cancer radiotherapy. *Curr Mol Pharmacol.* 2020;13(1):31–40.
 99. Kanzawa T, et al. Role of autophagy in temozolomide-induced cytotoxicity for malignant glioma cells. *Cell Death Differ.* 2004;11(4):448–57.
 100. O'Brien J, et al. Overview of MicroRNA biogenesis, mechanisms of actions, and circulation. *Front Endocrinol (Lausanne).* 2018;9:402.
 101. Sana J, et al. Risk Score based on microRNA expression signature is independent prognostic classifier of glioblastoma patients. *Carcinogenesis.* 2014;35(12):2756–62.
 102. Hayes J, et al. Prediction of clinical outcome in glioblastoma using a biologically relevant nine-microRNA signature. *Mol Oncol.* 2015;9(3):704–14.
 103. Niyazi M, et al. A 4-miRNA signature predicts the therapeutic outcome of glioblastoma. *Oncotarget.* 2016;7(29):45764–75.
 104. Unger K, et al. Improved risk stratification in younger IDH wild-type glioblastoma patients by combining a 4-miRNA signature with MGMT promoter methylation status. *Neurooncol Adv.* 2020;2(1):vdaa137.
 105. Weller M, et al. MGMT promoter methylation in malignant gliomas: ready for personalized medicine? *Nat Rev Neurol.* 2010;6(1):39–51.
 106. Giansanti P, et al. Mass spectrometry-based draft of the mouse proteome. *Nat Methods.* 2022;19(7):803–11.
 107. Lozinski M, et al. Transcriptomic profiling of DNA damage response in patient-derived glioblastoma cells before and after radiation and temozolomide treatment. *Cells.* 2022;11(7):1215.
 108. Hannen R, et al. Comparative transcriptomic analysis of temozolomide resistant primary GBM stem-like cells and recurrent GBM identifies up-regulation of the carbonic anhydrase CA2 gene as resistance factor. *Cancers (Basel).* 2019;11(7):921.
 109. de Jong Y, et al. Radiotherapy resistance in chondrosarcoma cells; a possible correlation with alterations in cell cycle related genes. *Clin Sarcoma Res.* 2019;9:9.
 110. Schoetz U, et al. Early senescence and production of senescence-associated cytokines are major determinants of radioresistance in head-and-neck squamous cell carcinoma. *Cell Death Dis.* 2021;12(12):1162.
 111. Qi XS, et al. Radioresistance of the breast tumor is highly correlated to its level of cancer stem cell and its clinical implication for breast irradiation. *Radiother Oncol.* 2017;124(3):455–61.
 112. Kocakavuk E, et al. Radiotherapy is associated with a deletion signature that contributes to poor outcomes in patients with cancer. *Nat Genet.* 2021;53(7):1088–96.
 113. de Mey S, Dufait I, De Ridder M. Radioresistance of human cancers: clinical implications of genetic expression signatures. *Front Oncol.* 2021;11: 761901.
 114. Hsu JB, et al. Identification of differentially expressed genes in different glioblastoma regions and their association with cancer stem cell development and temozolomide response. *J Pers Med.* 2021;11(11):1047.
 115. Wang M, Master SR, Chodosh LA. Computational expression deconvolution in a complex mammalian organ. *BMC Bioinformatics.* 2006;7:328.
 116. Cleator SJ, et al. The effect of the stromal component of breast tumours on prediction of clinical outcome using gene expression microarray analysis. *Breast Cancer Res.* 2006;8(3):R32.
 117. Chen X, et al. Relapse pathway of glioblastoma revealed by single-cell molecular analysis. *Carcinogenesis.* 2018;39(7):931–6.
 118. Kim EL, et al. Intratumoral heterogeneity and longitudinal changes in gene expression predict differential drug sensitivity in newly diagnosed and recurrent glioblastoma. *Cancers (Basel).* 2020;12(2):520.
 119. Petterson SA, Sorensen MD, Kristensen BW. Expression profiling of primary and recurrent glioblastomas reveals a reduced level of pentraxin 3 in recurrent glioblastomas. *J Neuropathol Exp Neurol.* 2020;79(9):975–85.
 120. Zhang W, et al. A review of the three-dimensional cell culture technique: approaches, advantages and applications. *Curr Stem Cell Res Ther.* 2016;11(4):370–80.
 121. Birgersdotter A, Sandberg R, Ernberg I. Gene expression perturbation in vitro—a growing case for three-dimensional (3D) culture systems. *Semin Cancer Biol.* 2005;15(5):405–12.
 122. Storch K, et al. Three-dimensional cell growth confers radioresistance by chromatin density modification. *Cancer Res.* 2010;70(10):3925–34.
 123. Vasileva NS, et al. Transcriptome changes in glioma cells cultivated under conditions of neurosphere formation. *Cells.* 2022;11(19):3106.

Publisher's Note

Springer Nature remains neutral with regard to jurisdictional claims in published maps and institutional affiliations.

Ready to submit your research? Choose BMC and benefit from:

- fast, convenient online submission
- thorough peer review by experienced researchers in your field
- rapid publication on acceptance
- support for research data, including large and complex data types
- gold Open Access which fosters wider collaboration and increased citations
- maximum visibility for your research: over 100M website views per year

At BMC, research is always in progress.

Learn more biomedcentral.com/submissions

